12-7-2020

Role of interplay of austenite and martensite phase fractions on the magnetocaloric and magnetoresistance effects across the martensite transition in $Ni_{45}Mn_{44}Sn_7In_4$Heusler alloy near room temperature

T. Chabri

Kartik Ghosh
Missouri State University

D. Mukherjee

T. K. Nath

Recommended Citation

Chabri, T., Kartik Ghosh, D. Mukherjee, and T. K. Nath. "Role of interplay of austenite and martensite phase fractions on the magnetocaloric and magnetoresistance effects across the martensite transition in Ni45Mn44Sn7In4 Heusler alloy near room temperature." Journal of Applied Physics 128, no. 21 (2020): 215106.

Journal of Applied Physics

Role of interplay of austenite and martensite phase fractions on the magnetocaloric and magnetoresistance effects across the martensite transition in $Ni_{45}Mn_{44}Sn_7In_4$ Heusler alloy near room temperature

Cite as: J. Appl. Phys. **128**, 215106 (2020); https://doi.org/10.1063/5.0028144
Submitted: 03 September 2020 . Accepted: 10 November 2020 . Published Online: 02 December 2020

T. Chabri, Kartik Ghosh, D. Mukherjee, and T. K. Nath

Journal of Applied Physics ARTICLE scitation.org/journal/jap

Role of interplay of austenite and martensite phase fractions on the magnetocaloric and magnetoresistance effects across the martensite transition in $Ni_{45}Mn_{44}Sn_7In_4$ Heusler alloy near room temperature

Cite as: J. Appl. Phys. **128**, 215106 (2020); doi: 10.1063/5.0028144
Submitted: 3 September 2020 · Accepted: 10 November 2020 ·
Published Online: 2 December 2020

T. Chabri,[1,2,a)] Kartik Ghosh,[3] D. Mukherjee,[1] and T. K. Nath[2]

AFFILIATIONS

[1]School of Physical Sciences, Indian Association for the Cultivation of Science, Kolkata 700032, West Bengal, India
[2]Department of Physics, Indian Institute of Technology Kharagpur, Kharagpur 721302, West Bengal, India
[3]Department of Physics, Astronomy, and Materials Science and the Center for Applied Science and Engineering, Missouri State University, Springfield, Missouri 65897, USA

[a)]**Author to whom correspondence should be addressed:** tanmaychabri@gmail.com

ABSTRACT

The influence of martensite and austenite phase fractions on the magnetocaloric and magnetoresistance (MR) properties has been studied across the first-order magneto-structural martensite transition in the polycrystalline $Ni_{45}Mn_{44}Sn_7In_4$ Heusler alloy near room temperature. Here, we have studied in detail the structural, calorimetric, magnetic, magnetocaloric, and magneto-resistance properties of the $Ni_{45}Mn_{44}Sn_7In_4$ Heusler alloy. The detailed investigation of thermal and magnetic field path dependent magnetization and resistivity reveals that In incorporation in the alloy increases the martensite transition (MT) temperature, magnetocaloric effect (MCE), and MR properties of the sample at relatively low magnetic fields near the room temperature. The temperature and magnetic field path dependent austenite phase fraction have been calculated using a theoretical model. A strong correlation between observed MR and field induced austenite phase fraction (f_{FIA}) has been established, which reveals that MR does not depend on the parent austenite and martensite phases. This work explores the fundamental phenomena of the interplay of austenite and martensite phase fractions that contribute to the magnetocaloric effect (MCE) and MR properties in In doped Ni-Mn-Sn compounds very close to room temperature. The maximum MR is found to be −36.2% for the change in the 8 T magnetic field, when f_{FIA} is 73.9% at 313 K. The isothermal magnetic entropy change, refrigeration capacity, and adiabatic temperature change are found to be 17.5 J kg^{-1} K^{-1}, 100.8 J/kg, and −7.2 K, respectively, for the change in the 5 T magnetic field near 315 K.

I. INTRODUCTION

Magnetic refrigeration based on the magnetocaloric effect (MCE) has drawn considerable research attention due to its potential role in replacing the conventional vapor-compression cooling technology with environment friendly and highly efficient solid-state cooling devices.[1] The cooling efficiency of a magnetic material being used as a magnetic refrigerant depends primarily on three parameters, namely, the adiabatic temperature change (ΔT_{ad}), the isothermal magnetic entropy change (ΔS_M), and the refrigeration capacity (RC), which define the amount of heat that can be transferred from the cold end to the hot end in a refrigeration cycle.[2] For practical device applications, the parameters defining the cooling efficiency of the materials should be high at low magnetic fields near room temperature. In the earlier stages, magnetocaloric refrigeration technology was restricted to the adiabatic demagnetization in the vicinity of second-order magnetic

transitions in magnetic materials; however, currently, adiabatic magnetization (inverse MCE) is also exploited for magnetocaloric cooling, where magnetic entropy increases with the application of a magnetic field.[3,4] The inverse MCE is observed in material systems, where the first-order phase transitions occur, such as anti-ferromagnetic (AF) → ferromagnetic (FM) ($Fe_{0.49}Rh_{0.51}$),[5] AF-collinear → AF-noncollinear (Mn_5Si_3),[3] or anti-ferromagnetic → ferrimagnetic ($Mn_{1.82}V_{0.18}Sb$).[4] It is known that the presence of mixed magnetic exchange interactions among the different co-existing magnetic phases in these systems leads to further spin disorder with the application of external magnetic fields, which increases the configurational magnetic entropy and the ensuing MCE in these materials.[3,6] Rare earth Gd and various manganites (e.g., $La_{0.67}Ca_{0.33-x}Sr_xMnO_3$) show MCE near their second-order magnetic phase transitions.[7,8] However, some intermetallic compounds, such as La–Fe–Si,[9,10] Gd–Si–Ge,[11] Mn–Fe–P–As,[12] and Ni–Mn-based Heusler alloys[13,14] having first-order phase transitions show giant inverse MCE near their transitional temperatures with respect to the materials showing second-order magnetic transition. Among them, the Ni–Mn–Z (Z = Sn, In, Sb) Heusler alloy systems have drawn considerable attention due to their significant MCE along with their low cost of raw materials and easy fabrication as compared to the rare-earth element based compounds.[15–17] The flexibility in controlling the transition temperature with the variation of Z elements and compositions makes these alloys much interesting in the field of magnetic refrigeration.[17–19] These Ni–Mn–Z (Z = Sn, In, Sb) alloys show magnetic field induced first order martensite transition (MT) that occurs between a FM austenite and a low magnetization martensite phase, which may be paramagnetic, anti-ferromagnetic, or ferrimagnetic.[20–23] The large difference in magnetization across the MT strongly influences the thermodynamics of the transition to be controlled by an external magnetic field. The MT, being first-order in nature, strongly depends on thermal (heating and cooling) and magnetic field (increasing and decreasing field) paths. As a result, the phase fractions of the austenite phase (high magnetization and low resistivity) and the martensite phase (low magnetization and high resistivity) across MT strongly depends on thermal and magnetic field paths, which have direct consequences on the observed MCE and magneto-resistance (MR) properties.[24,25] So, the synthesis of new materials by varying compositions and elements is not only a possible solution for finding large MCE and MR, but a route to manipulate these properties for existing compounds is also equally important from the application point of view. Depending on thermal and magnetic field path history, resistivity and magnetization change across the MT for a particular temperature and magnetic field can be exploited as giant magneto-resistance (GMR) effect[2,26] and giant MCE,[19,24] respectively, having great potential in technological applications. However, the inherent thermal and magnetic hysteresis losses across MT pose the real obstacle toward the reversibility of large entropy changes in practical applications.[27] Therefore, the hysteresis loss is a crucial parameter, which can compromise the MCE and MR properties of the sample. In this context, among various Ni–Mn based Heusler alloy, off-stoichiometric Ni–Mn–Sn Heusler alloys have drawn considerable attention due to their high inverse MCE and giant MR with relatively small thermal and magnetic hysteresis loss across MT near the room temperature.[13,24,26,28,29] Moreover, in these off-stoichiometric Ni–Mn–Sn Heusler alloys, the first-order MT and second-order magnetic transitions occur simultaneously but with different temperature regimes.[30] As maximum MCE can be obtained when these two transition temperatures lie close to each other,[6] it is one of the preliminary goals in designing novel materials to make these two transition temperatures close to each other.[30] In this context, we have chosen $Ni_{45}Mn_{44}Sn_7In_4$ Heusler alloy as a possible potential material, which is expected to show high MCE and large MR for the following reasons. In our previous work, we have shown that large ΔS_M (15 J kg^{-1} K^{-1}) and ΔT_{ad} (−5.1 K) have been observed below room temperature (275 K) for the $Ni_{45}Mn_{44}Sn_{11}$ Heusler alloy sample for the change in the 5 T magnetic field.[13] A large field induced change in the resistivity is also observed for the same composition at 270 K.[14] Guo *et al.* also confirmed that In doping at the Sn site increases the symmetry of the martensite phase, MT temperature, and the magnetocaloric properties of the sample.[31] So, we wished to add a small amount of In in $Ni_{45}Mn_{44}Sn_{11}$ at the Sn site, expecting large MCE and MR near room temperature.

In this article, we have thoroughly investigated the structural, calorimetric, magnetic, magnetocaloric, and magneto-resistance properties of the $Ni_{45}Mn_{44}Sn_7In_4$ Heusler alloy. It has been observed, comparing with our previous work, that In addition increases the MT temperature, MCE, and MR properties of the sample at relatively low magnetic fields near the room temperature. The detailed investigation of thermal and magnetic field path dependent magnetization and resistivity reveals that the austenite and martensite phase fraction in the vicinity of MT is highly dependent on magnetic field and temperature. The fraction of the metastable martensite phase inside MT, which can be converted to the austenite phase by the application of a magnetic field only at the isothermal condition, has been calculated using a theoretical model. The relation between the observed MR and field induced austenite phase fraction (f_{FIA}) has been established, which confirms that MR of the sample does not depend on the parent austenite and martensite phases and depends only on f_{FIA}. This work explores the fundamental phenomena of the interplay of austenite and martensite phase fractions that contribute to MCE and MR properties in In doped Ni–Mn–Sn compounds very close to room temperature.

II. EXPERIMENTAL DETAILS

The polycrystalline $Ni_{45}Mn_{44}Sn_7In_4$ Heusler alloy sample is prepared using elemental Ni, Mn, Sn, and In (99.99%) by an arc melting process in an inert Ar atmosphere. The pure elements before melting and the bulk ingot after melting were weighed. Negligible weight loss was observed after the sample preparation and the real composition of the prepared sample was assumed to be the same as the nominal one. The as grown $Ni_{45}Mn_{44}Sn_7In_4$ ingot was sealed in a quartz tube under the pressure of 10^{-5} mbar and annealed at 1273 K for 24 h in a tube furnace. After annealing, the ingot was quenched in ice water. The ingot was cut into pieces by a diamond cutter for experiments to probe different physical properties. The crystal structure of the sample was investigated at room temperature by using a high resolution x-ray diffractometer

(HRXRD, Philips PANalytical X'Pert PRO) using CuKα radiation ($\lambda = 1.542$ Å). The chemical characterization of the sample at room temperature was carried out by using a photoelectron spectrometer (XPS, PHI 5000Versa Probe II). Elemental composition was checked by the energy dispersive analysis of x-ray (EDAX). The calorimetric property of the sample was probed by a commercial calorimeter (Mettler Toledo) in the temperature range of $222\ \text{K} \leq \text{T} \leq 423\ \text{K}$ with a typical heating and cooling rate of 10 K/min. The temperature and DC magnetic field dependent magnetization measurements were carried out using a commercial vibrating magnetometer (Quantum Design). Isofield magnetization data have been recorded with the variation of temperature at zero field cooled (ZFC), field cooled cooling (FCC), and field cooled warming (FCW) modes at different magnetic fields. The rate of increase and decrease in the temperature was 10 K/min. At the ZFC mode, the sample is initially cooled from 400 K to 5 K in the absence of the magnetic field and then a 0.05 T magnetic field was applied and data were recorded at the time of heating up to 350 K. After that, the data were collected at the time of cooling, producing FCC branch, without removing the magnetic field. At the last step, data were recorded producing FCW branch keeping the sample with the magnetic field on. Isothermal magnetic field dependent magnetization (M–H) data were recorded at different temperatures in the vicinity of MT, by varying the magnetic field from 0 T to 5 T. Isofield (at 0 T and 8 T) and isothermal (at 200 K, 245 K, 275 K, 295 K, and 313 K) electronic transport measurements were carried out by using a home-made four probe resistivity setup using a low temperature high field superconducting magnet from Oxford Instruments (UK).

III. RESULTS AND DISCUSSION

Figures 1(a)–1(d) show the narrow scan XPS spectra for Ni, Mn, Sn, and In elements, respectively, of the $Ni_{45}Mn_{44}Sn_7In_4$ Heusler alloy. The observed binding energies for Ni $2p_{3/2}$, Mn $2p_{3/2}$, Sn $3d_{5/2}$, and In $3d_{5/2}$ peaks are 852.1 eV, 639.0 eV, 484.6 eV, and 443.6 eV, respectively. On the other hand, the Ni $2p_{1/2}$, Mn $2p_{1/2}$, Sn $3d_{3/2}$, and In $3d_{3/2}$ peaks appear at 869.4 eV, 648.7 eV, 493.0 eV, and 451.2 eV, respectively. For Ni, the core level $2p_{3/2}$ and $2p_{1/2}$ are accompanied by $2p_{3/2}$ and $2p_{1/2}$ satellite peaks at 858.5 eV and 874.1 eV, respectively.[13] The recorded binding energies appear at the respective positions of metallic states, thereby confirming that the elements are not oxidized after melting under Ar atmosphere.[26]

The peaks of the room temperature XRD pattern, shown in Fig. 2, are indexed as a tetragonal $L1_0$ structure which confirms that the $Ni_{45}Mn_{44}Sn_7In_4$ alloy is in pure martensite phase at room temperature similar to the previous report on the $Ni_{41}Mn_{50}Sn_9$ ternary alloy.[32] In our previously reported works, we have showed that the $Ni_{45}Mn_{44}Sn_{11}$ and $Ni_{45}Mn_{44}Sn_9In_2$ Heusler alloys are in the pure austenite phase and mixed phase (cubic austenite + tetragonal), respectively, at room temperature.[13,26] It implies that martensite transition temperature increases with the addition of In at the Sn position. The inset of Fig. 2 shows the EDAX spectrum of the $Ni_{45}Mn_{44}Sn_7In_4$ Heusler alloy. The peaks of Ni, Mn, Sn, and In elements are observed at their respective energy positions. The wt.% of the constituting elements are found to be Ni ~ 45.02%, Mn ~ 43.90%, Sn ~ 7.10%, and In ~ 3.98%, thereby confirming that the actual composition of the prepared sample is nearly the same with the nominal composition.

Figure 3(a) shows the heat flow in the sample as a function of temperature during heating and cooling in the absence of the magnetic field. Large exothermic and endothermic peaks at 301.9 K and 322.1 K, respectively, have been observed during cooling and heating, which correspond to the direct martensite transition and reverse martensite transition temperatures, respectively. The martensite transition is characterized by martensite start temperature (M_S) and martensite finish temperature (M_F), whereas the reverse martensite transition is characterized by austenite start temperature (A_S) and austenite finish temperature (A_F). Above M_S, the sample is in the pure austenite phase. When the temperature of the sample starts to decrease, the martensite phase starts to evolve at M_S across the martensite transition regime at the expense of the austenite phase, and the conversion of the austenite phase into the martensite phase is finished at M_F. After that, the sample is in the pure martensite phase. So, between M_S and M_F, both phases coexist in the sample. The opposite phenomenon has been observed on heating. At A_S, the austenite phase starts to increase, and at A_F, the sample is in the pure austenite phase. The characteristic temperatures (M_S, M_F, A_S, and A_F) of the martensite and reverse martensite transition are determined from the intersection of the tangent line with the largest slope of the DSC peak and baseline. From Fig. 3(a), the characteristics temperatures are determined to be $M_S = 315.6 \pm 0.2$ K, $M_F = 293.5 \pm 0.2$ K, $A_S = 308.6 \pm 0.2$ K, and $A_F = 329.8 \pm 0.2$ K. It has been observed that M_S and A_F, i.e., the temperatures above which the sample is in the austenite phase, are not equal for cooling and heating paths. A similar phenomenon has been observed for M_F and A_S. So, a thermal hysteresis occurs between martensite transition and reverse martensite transition, thereby confirming the first-order nature of the transition. From the analysis of the DSC data shown in Fig. 3(a), it is confirmed that MT in the sample is very close to the room temperature. As Ni–Mn based Heusler alloys are magnetic in nature, the total entropy of the $Ni_{45}Mn_{44}Sn_7In_4$ Heusler alloy system is the summation of magnetic entropy (ΔS_M), lattice entropy (S_l), and electronic entropy (S_e),

$$S_{Total}(T,\ H) = \Delta S_M + S_l + S_e = \Delta S_M + S(T, H = 0), \qquad (1)$$

where $S(T,\ H = 0) = S_l + S_e$, which can be approximated to be independent of the magnetic field and entirely depends on the temperature of the sample. We have calculated $S(T,\ H = 0)$ from calorimetric data after subtracting baseline correction, using the following relation:[33]

$$S(T,\ H = 0) = \int_{A_S}^{T} \frac{1}{T}\left(\frac{dQ}{dT}\right) dT, \qquad (2)$$

where $dQ/dT = (dQ/dt)/(dT/dt)$. Figure 3(b) shows $S(T,\ H = 0)$ vs T across the martensite transition. The changes in the thermal entropies are found to be 46.2 J kg^{-1} K^{-1} and 44.1 J kg^{-1} K^{-1} for direct martensite transition and reverse martensite transition during cooling and heating, respectively. The temperature ranges across which thermal entropy changes occur are different for cooling and

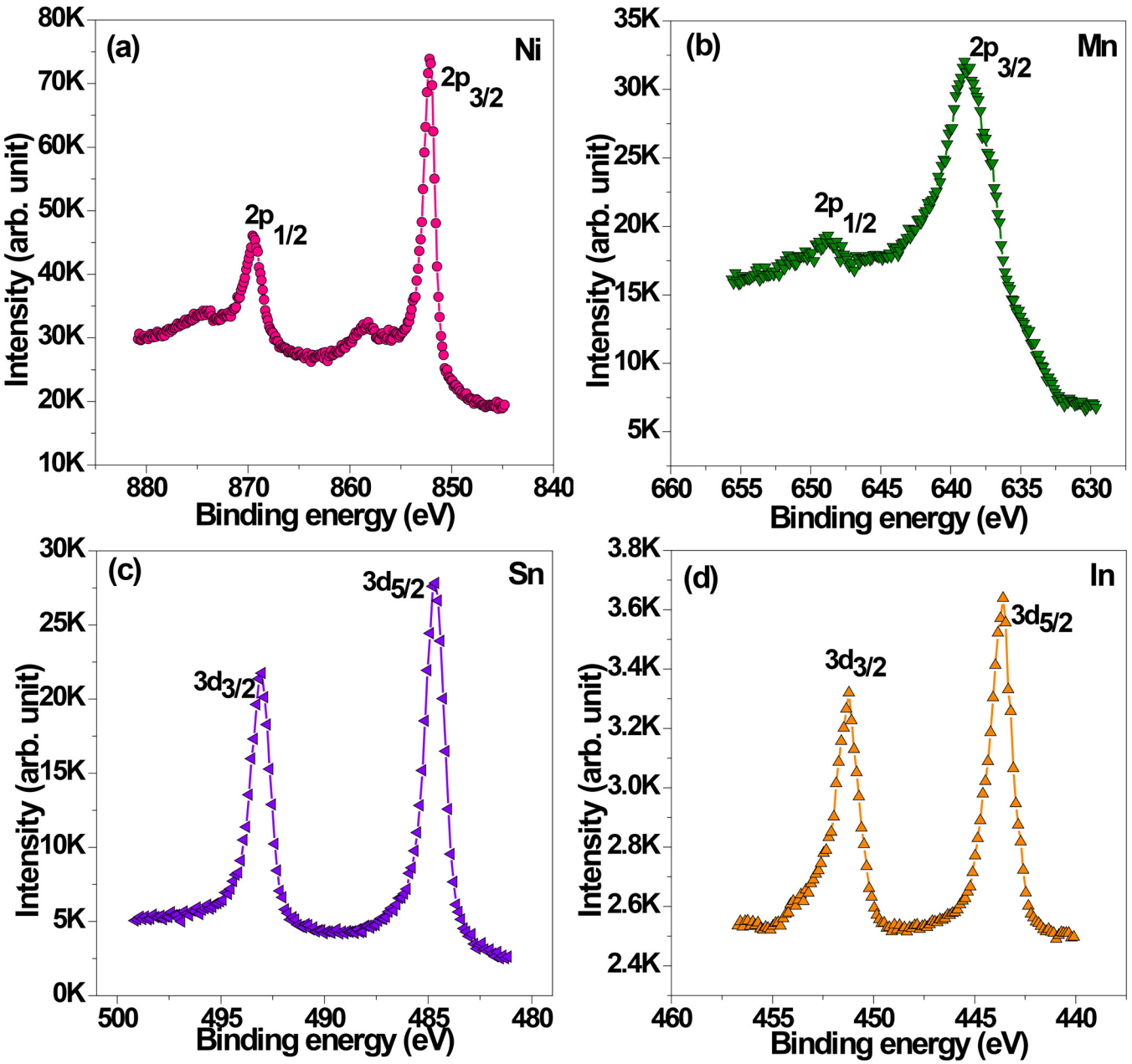

FIG. 1. (a)–(d) Narrow scan XPS Spectra for Ni, Mn, Sn, and In elements, respectively, in the $Ni_{45}Mn_{44}Sn_7In_4$ Heusler alloy at room temperature.

heating due to the thermal hysteresis in the direct and reverse MT. The changes of enthalpy (ΔH) across the martensite transition are calculated using the following relation:[33]

$$\Delta H = \int_{T_i}^{T_f} \frac{1}{T}\left(\frac{dQ}{dT}\right)\left(\frac{dT}{dt}\right)^{-1} dT \qquad (3)$$

and are found to be $\Delta H_c = 14.2$ J/g (on cooling) and $\Delta H_h = 14.1$ J/g (on heating) for direct martensite transition and reverse martensite transition, respectively. Chabri *et al.* also calculated the change in the enthalpy for the $Ni_{45}Mn_{44}Sn_{10}Al_1$ Heusler alloy and the values of ΔH_c and ΔH_h are found to be 15.8 J/g and 15.0 J/g, respectively.[2] So, the enthalpy of our present sample is slightly smaller than that of the $Ni_{45}Mn_{44}Sn_{10}Al_1$ Heusler alloy.

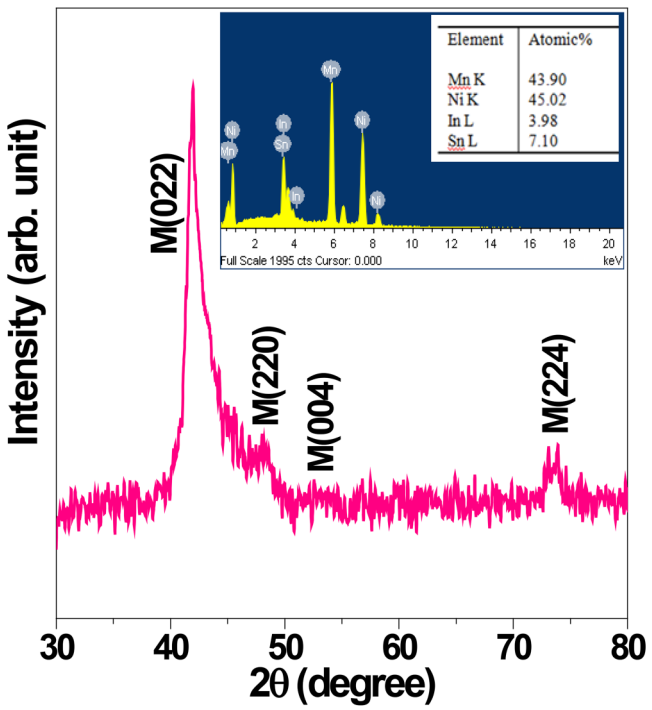

FIG. 2. X-ray diffraction pattern of $Ni_{45}Mn_{44}Sn_7In_4$ Heusler alloy recorded at room temperature. Inset: EDAX spectrum of the $Ni_{45}Mn_{44}Sn_7In_4$ Heusler alloy.

Figure 4(a) shows the isofield thermomagnetization data at the magnetic field of 0.05 T under ZFC, FCC, and FCW modes for the $Ni_{45}Mn_{44}Sn_7In_4$ Heusler alloy in the temperature range of 10–350 K. On cooling under the FCC mode from 350 K, the magnetization of the sample increases due to the paramagnetic (PM) → ferromagnetic (FM) transition near the Curie temperature of the austenite phase (T_C^A). In the immediate vicinity of it, the magnetization of the sample suddenly decreases across the martensite transition up to M_F, at which the sample is in the pure martensite phase. This happens due to the conversion of the FM austenite phase into the weak magnetic martensite phase. With a further decrease in the temperature, the magnetization of the sample remains nearly the same between 200 and 300 K and suddenly increases near the Curie temperature of the martensite phase (T_C^M) due to the FM transition in the martensite phase. The magnetization in the FCW mode follows the same curve of the FCC mode, except the martensite transition regime. A thermal hysteresis in magnetization is observed between FCC and FCW modes near the martensite transition, thereby confirming its first-order nature. The inset of Fig. 4(a) shows the zoomed view of the thermomagnetization data in the temperature range of 290–330 K near the MT. The width of thermal hysteresis is found to be 8.1 K, and it is calculated by taking the temperature difference of the middle points of the direct martensite transition and reverse martensite transition. However, the transitions near T_C^M and T_C^A are of second-order in nature. The characteristic temperatures of martensite transition, M_S, M_F, A_S, and A_F (defined in the calorimetric part) are also shown in the inset of Fig. 4(a) and are found to be 314.4 K, 302.5 K, 310.8 K, and 320.4 K, respectively. A_S and M_F are calculated from the intersection of the tangent line of the largest slope and baseline of $M(T)$ curves. The values of T_C^M and T_C^A are determined from the minima of dM/dT vs T curves and are found to be 128.1 K and 320.0 K, respectively (see Fig. S1 in the supplementary material). On heating under the ZFC mode, initially, magnetization increases with temperature. This happens due to the unlocking of moments frozen at low temperatures. As a result, unlocked moments can easily align along the applied magnetic field and magnetization increases. The sudden increase in magnetization across the reverse martensite transition (or decrease in magnetization across the direct martensite transition) happens due to the exchange interaction between Mn atoms, sitting at the regular Mn site and the excess Mn atoms in Ni and Sn sites.[34] These excess Mn atoms play a crucial role in the sample undergoing the martensite transition due to the destabilization of the cubic austenite phase against tetragonal distortion in the martensite phase.[34]

It has been observed that various aspects of martensite transition, e.g., magnetic field dependent shift of MT, broadening of the transition region, thermal and magnetic paths' dependence of magnetoresistance, and magnetic entropy, depend on chemical compositions and disorder.[24,31,35] Here, we define the direct martensite transition temperature (T_{AM}) and reverse martensite transition temperature (T_{MA}) as temperatures, where the first-order derivative of FCC and FCW curves show peaks near the martensite transition and reverse martensite transition, respectively. It has been observed that T_{AM} can be controlled by varying the valence electron concentration (e/a) or substituting a new element at the Z position.[31,36] It is generally seen that T_{AM} increases with the increase in e/a.[15,33,37,38] In our previous studies, it was observed that T_{AM} for $Ni_{45}Mn_{44}Sn_{11}$[13] and $Ni_{45}Mn_{44}Sn_9In_2$[26] Heusler alloys are 264.8 K and 290 K, respectively. In our present study of the $Ni_{45}Mn_{44}Sn_7In_4$ alloy, T_{AM} is observed to be 310.2 K. So, T_{AM} shifts toward higher temperatures with the addition of In at the Sn site or decreasing the valence electron concentration ratio (e/a ratio). The valence electrons per atom are 10 ($3d^84s^2$), 7 ($3d^54s^2$), 4 ($5s^25p^2$), and 3 ($5s^25p^1$) for Ni, Mn, Sn, and In, respectively.[39] Figure 4(b) shows the variation of T_{AM} with e/a for $Ni_{45}Mn_{44}Sn_{11-x}In_x$ ($x = 0, 2, 4$). So, our result, i.e., negative dependence of T_{AM} with e/a ratio, contradicts with the general rule. Such anomaly has also been reported in several other cases, e.g., $Ni_{50}Mn_{25+x}Ga_{25-x}$,[40] $Co_{45}Ni_{25}Ga_{30}$ alloy systems,[41] where the martensite transition temperature decreases with increasing e/a ratio. This indicates that there may be other factors (except e/a ratio) which control T_{AM}. It has been proved that the martensite transition temperature can be changed with the variation of cell volume.[42] Guo *et al.* reported that the martensite transition increases with a decrease in the e/a ratio by the substitution of In in the Z site.[31] Aksoy *et al.* showed that the substitution of smaller Ga atoms at the In site in $Ni_{50}Mn_{34}In_{16-x}Ga_x$ increases T_{AM} rapidly.[43] So, we can conclude that, though e/a ratio decreases with the substitution of smaller In atoms at Sn positions, the decrease of cell volume with In addition is the possible reason for the increase in T_{AM} for the $Ni_{45}Mn_{44}Sn_{11-x}In_x$ ($x = 0, 2, 4$) Heusler alloy. From the inset of Fig. 4(a), it is observed that the martensite transition is broad due to the disorder present in the sample, though it is of first order by

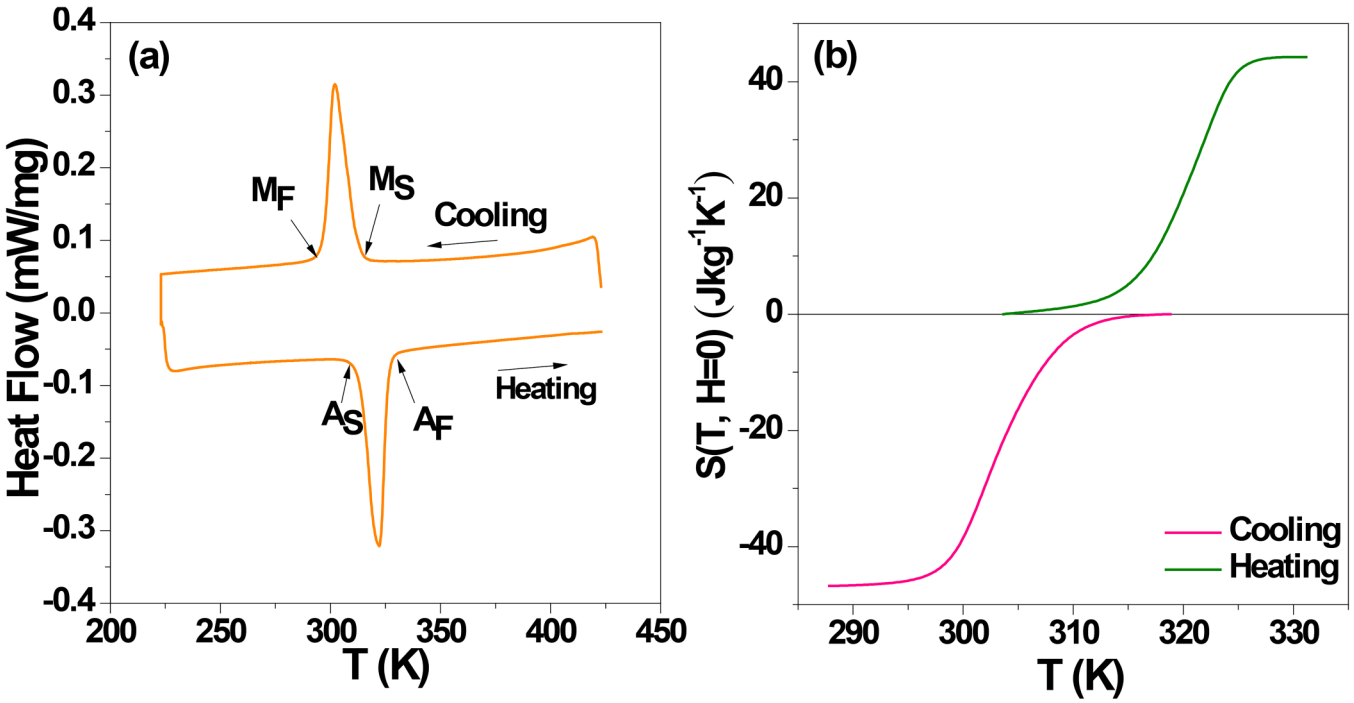

FIG. 3. (a) Heat flow vs temperature during heating and cooling in the absence of the magnetic field for the $Ni_{45}Mn_{44}Sn_7In_4$ Heusler alloy. (b) $S(T, H = 0)$ vs T across the martensite transition for heating and cooling paths.

nature. The chemical formula of the $Ni_{45}Mn_{44}Sn_7In_4$ alloy can be expressed as $[(Ni_{45}Mn_5)(Mn_{25})(Sn_7In_4Mn_{14})]$. So, the excess Mn atoms occupy the vacant Ni and Z sites of ordered $Ni_{50}Mn_{25}Z_{25}$. Bhobe *et al.* showed that a local disorder presents in the high temperature cubic austenite phase due to the presence of excess Mn atoms, which causes a change in the Ni–Sn and Ni–Mn bond lengths.[44] So, the $Ni_{45}Mn_{44}Sn_7In_4$ Heusler alloy has local disorder in Ni–Sn and Ni–Mn bond lengths, which is the possible reason for broad MT. The broadening of MT for the present $Ni_{45}Mn_{44}Sn_7In_4$ alloy has been calculated using the same protocol of our previous study.[26] From Fig. 4(c), it is observed that the broadening of the martensite transition for the applied magnetic field of 0.05 T is 9.0 K. However, the same is 6.0 K for the $Ni_{45}Mn_{44}Sn_9In_2$ Heusler alloy.[26] So, broadening of MT increases with the increase of In content, which is desirable from the application point of view. This signifies that intersite disorder is significant for the $Ni_{45}Mn_{44}Sn_7In_4$ Heusler alloy with respect to $Ni_{45}Mn_{44}Sn_9In_2$ Heusler alloy.[26] Another important feature of martensite transition is magnetic field dependence of MT. Figure 4(d) shows thermomagnetization curves for FCC and FCW modes near MT at 1 T, 3 T, and 5 T magnetic fields. It is observed that the hysteresis loops shift toward lower temperatures with the increase in the magnetic field. T_{AM} and T_{MA} are estimated from the first order derivative of $M(T)$ curves (see Fig. S2 in the supplementary material). The left and right axes of the inset of Fig. 4(d) show the variation of T_{AM} and T_{MA}, respectively, with the magnetic field. The rate of decrease in T_{AM} and T_{MA} with the magnetic field is 1 K/T. The decrease in the martensite transition temperature happens due to the formation of the single variant austenite phase from the modulated twinned martensite phase with the increase in the magnetic field. As a consequence, the highly order cubic austenite phase stabilizes at low temperatures with the increase in the magnetic field.

Isothermal field dependent magnetization curves, shown in Fig. 5(a), have been recorded for several temperatures for the $Ni_{45}Mn_{44}Sn_7In_4$ Heusler alloy in the temperature range from 290 K to 350 K up to 5 T magnetic field for field increasing and decreasing paths. It has been clearly observed that the isothermal magnetization increases gradually with the magnetic field up to 3 T magnetic field at 308 K, 310 K, 312 K, 314 K, 315 K, and 318 K. After that, the slope of the isothermal M–H increases with the increasing magnetic field. This occurs due to the field induced magneto-structural transformation of the low magnetization martensite phase into the high magnetization austenite phase at a particular temperature. This phenomenon is not observed for isothermal M–H curves, when the temperature is below (300 K and 306 K) and above (320 K, 330 K, and 350 K) MT temperature. So, it is confirmed that a magnetic field induced transition occurs only inside the MT regime. Meta-magnetic behavior characterized by a sudden increase in magnetization with a small change in the external applied magnetic field and the magnetic hysteresis between field increasing and decreasing paths have been noticed when the

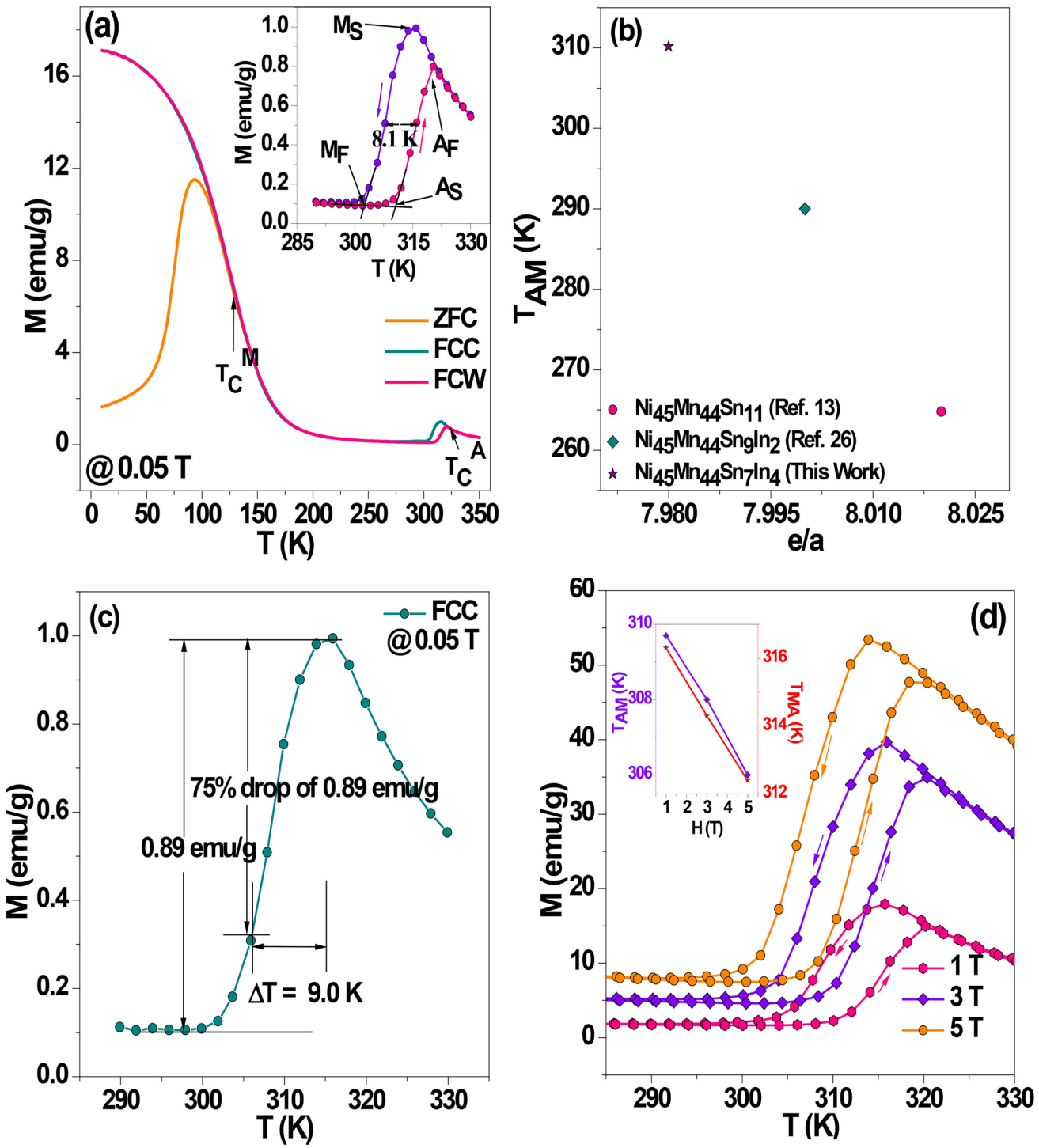

FIG. 4. (a) Isofield thermo-magnetization data at 0.05 T for ZFC, FCC, and FCW modes of the $Ni_{45}Mn_{44}Sn_7In_4$ Heusler alloy. Inset: zoomed view of the thermo-magnetization data for FCC and FCW modes near the martensite transition regime. (b) Variation of T_{AM} with *e/a* for $Ni_{45}Mn_{44}Sn_{11-x}In_x$ (x = 0, 2, 4). (c) Broadening of the direct martensite transition from the thermo-magnetization curve at 0.05 T of the $Ni_{45}Mn_{44}Sn_7In_4$ Heusler alloy. (d) Shift of thermo-magnetic hysteresis loops near the MT regime at 1 T, 3 T, and 5 T magnetic field. Inset: variation of T_{AM} and T_{MA} with magnetic field.

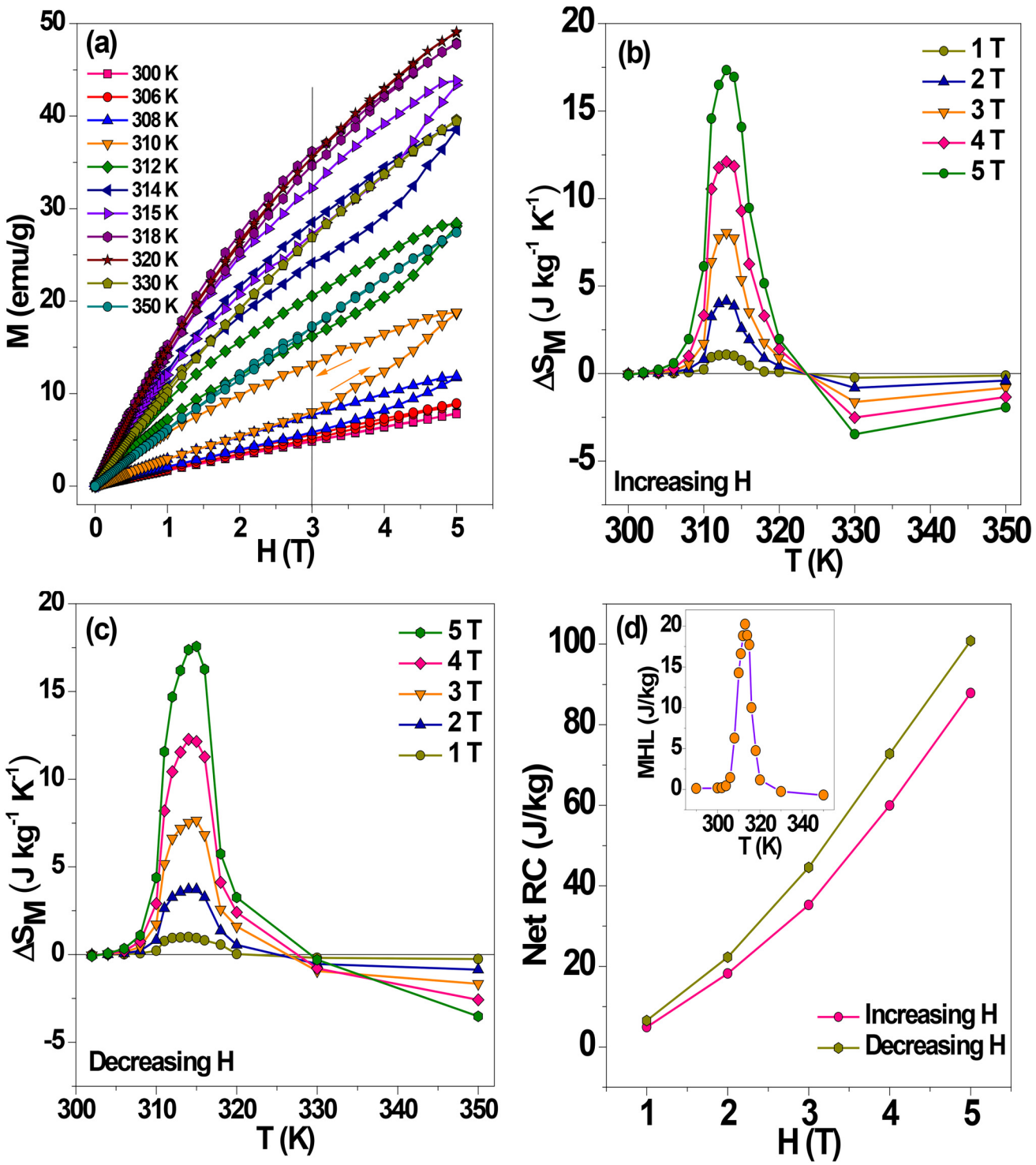

FIG. 5. (a) Isothermal *M–H* curves at several temperatures in the vicinity of the martensite transition regime in the first quadrant for field increasing and decreasing paths. (b) ΔS_M vs T for different magnetic fields, calculated from increasing field *M–H* data. (c) ΔS_M vs T for different magnetic fields, calculated from decreasing field *M–H* data. (d) Net RC vs H calculated from Figs. (b) and (c). Inset: variation of magnetic hysteresis loss with temperature for the change of 5 T magnetic field.

temperature of the sample is inside MT. The magnetic field increasing path has lower magnetization compared to the field decreasing path at a particular magnetic field. This confirms that, when the magnetic field is decreased from a maximum applied field, the low magnetization martensite phase does not transform back by the same amount. As a result, the field decreasing path has a higher fraction of the high magnetization austenite phase at a particular field than field increasing path. The difference in magnetization (ΔM) between increasing and decreasing magnetic field at a particular magnetic field is larger, when the sample temperature is inside MT (see Fig. S3 in the supplementary material). ΔM appears to be maximum at 3.7 T, i.e., after 3 T beyond which field induced transition triggers. As observed from isothermal M–H curves [Fig. 5(a)], the difference of magnetization between two consecutive isotherms increases inside the MT regime. So, we can expect large change in magnetic entropy in the vicinity of the martensite transition regime. The magnetic field induced isothermal entropy change (ΔS_M) has been estimated by the following Maxwell's relation:[45]

$$\Delta S_M = \int_0^H \left(\frac{\partial M}{\partial T}\right)_H dH. \tag{4}$$

So, the sign of ΔS_M depends on the slope of the M–T curve, which is positive and negative near the first order martensite transition and second order FM → PM transition in the austenite phase, respectively. As a consequence, we get positive MCE (inverse MCE) and negative MCE (conventional MCE) at the respective temperature regime. However, the direct applications of Maxwell's relation for the first order transition including mixed states without following precautions may lead to the wrong results in ΔS_M calculations.[46,47] ΔS_M can be overestimated for the systems having multiphase.[48] Caron *et al.* showed that one can accurately calculate the ΔS_M value, when Maxwell's equation is used to the isothermal M–H curves, obtained by a loop protocol.[49] In this process, the respective temperature to record isothermal M–H data is always reached by cooling the sample from the temperature, where the sample is in a paramagnetic state. Figures 5(b) and 5(c) show the variation of isothermal magnetic entropy change for different magnetic fields, calculated from increasing and decreasing field of isothermal M–H curves, respectively. It is observed that maximum values of ΔS_M are found to be 17.3 J kg^{-1} K^{-1} and 17.5 J kg^{-1} K^{-1}, calculated from increasing and decreasing field paths of M–H data, respectively, for the change in the magnetic field of 5 T at 314 K, which is very close to room temperature. So, the ΔS_M values are found to be nearly the same for the application and withdrawal of the magnetic field. This signifies that this material can take out the same amount of heat for the application and withdrawal for the same amount of magnetic field. It is observed that the maximum ΔS_M increases with the increase in the magnetic field. In our previous studies, we have seen that maximum ΔS_M values are found to be 15 J kg^{-1} K^{-1} and 17 J kg^{-1} K^{-1} for $Ni_{45}Mn_{44}Sn_{11}$ and $Ni_{45}Mn_{44}Sn_9In_2$, respectively, for the change in the magnetic field of 5 T, calculated from field increasing isothermal M–H data.[13,26] So, it can be concluded that ΔS_M is increased slightly with the increase in the In content at Sn sites. Though, high isothermal magnetic entropy change is one of the desired characteristics for a magnetocaloric material, high refrigerant capacity (RC), negligible hysteresis loss, and large adiabatic temperature change are also the other parameters, which decide the potentiality of the material as a magnetic refrigerant. Quantitatively, RC is the area under the ΔS_M vs T curve within full width at half maxima (FWHM) and can be calculated using the following formula:

$$RC = \int_{T_{Cold}}^{T_{Hot}} |-\Delta S_M| dT, \tag{5}$$

where T_{Hot} and T_{Cold} is the higher and lower temperature of the FWHM of the ΔS_M vs T curve. The RC of a magnetic refrigerant, having first order MT, is constrained by dissipative magnetic hysteresis loss (MHL). Quantitatively, MHL is the area inside the field increasing and decreasing M–H curves.[24] The MHL is the loss of energy due to the reorientation of the structure from the modulated martensite phase to the cubic austenite phase due to the application of the magnetic field or vice versa. The inset of Fig. 5(d) shows the MHL vs temperature plot in the vicinity of the martensite transition. The maximum magnetic hysteresis loss is 20.2 J/kg at 313 K. The net RC has been calculated by subtracting the average field induced hysteresis loss from the calculated RC, using Eq. (5). Figure 5(d) shows the variation of the net RC with magnetic field, calculated from Figs. 5(b) and 5(c). The maximum values of net RC, calculated from Figs. 5(b) and 5(c), are 87.8 J/kg and 100.8 J/kg, respectively. The maximum value of net RC for the $Ni_{45}Mn_{44}Sn_9In_2$ Heusler alloy was 48 J/kg.[26] So, it can be concluded that RC increases with the increase in In at the Sn site. This happens due to the increase in FWHM of ΔS_M vs T curves with the increase in In.[26]

In addition to, ΔS_M and RC, the estimation of adiabatic temperature change (ΔT_{ad}) with the application of magnetic field concludes the efficacy of the material in the field of magnetic refrigeration. We have estimated adiabatic temperature change using the results of calorimetric measurement [$S(T, H = 0)$, which is the change of entropy due to lattice and electronic structure] and isothermal magnetic measurement [ΔS_M, which is the magnetic entropy change]. The total entropy of our magnetic Heusler alloy [$S(T, H)$] is calculated using Eq. (1). Then, we have plotted $S(T, H)$ and $S(T, H = 0)$ as a function of temperature in a same graph and followed a isentropic path (a line parallel to the T axis) from the zero field entropy curve [$S(T, H = 0)$] to the total entropy curve [$S(T, H)$], which satisfies the adiabatic condition. ΔT_{ad} with the application of the magnetic field can be estimated using the following equation:[50]

$$\Delta T_{ad}(H, T) = T(S, H) - T(S, 0), \tag{6}$$

where $T(S,H)$ and $T(S,0)$ are the temperatures of the sample in the presence and absence of the magnetic field with constant entropy, respectively. Figure 6 shows the variation of ΔT_{ad} with temperature for the application of the magnetic field of 5 T of the $Ni_{45}Mn_{44}Sn_7In_4$ Heusler alloy. The negative and positive ΔT_{ad} correspond to the inverse and conventional MCE, respectively. The

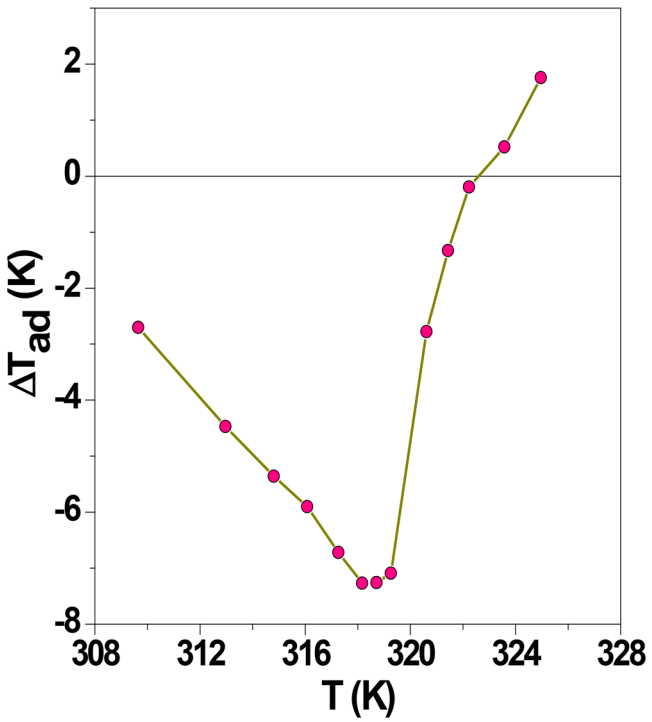

FIG. 6. ΔT_{ad} vs T in the vicinity of the martensite transition regime for the $Ni_{45}Mn_{44}Sn_7In_4$ Heusler alloy for the change in 5 T magnetic field.

maximum negative value is found to be −7.2 K at 318.1 K for the change in the 5 T magnetic field. This value of ΔT_{ad} is larger than our previously reported ΔT_{ad} of $Ni_{45}Mn_{44}Sn_{11}$ (−5.1 K) and $Ni_{45}Mn_{44}Sn_9In_2$ (−3.8 K) Heusler alloys.[13,26] The value of ΔT_{ad} is also larger than other Ni–Mn–Sn based Heusler alloy systems.[51,52] So, it can be concluded that In addition at Sn sites increases the value of ΔT_{ad}, which decides the potential application of the sample as a magnetic refrigerant. The values of MT temperature, ΔS_M, and ΔT_{ad} for $Ni_{45}Mn_{44}Sn_{11-x}In_x$ (x = 0, 2, 4) and other Heusler alloys in the vicinity of the martensite transition are summarized in Table I.

Figure 7(a) shows isofield temperature dependent resistivity [$\rho(T)$] data in the vicinity of the MT regime under the magnetic field of 0 T and 8 T for the $Ni_{45}Mn_{44}Sn_7In_4$ Heusler alloy. At first on cooling, the sample from 320 K, resistivity is observed to be the same up to 318.1 K. After that, resistivity increases suddenly with the decrease in the temperature up to 304 K. This happens due to the conversion of the low resistive austenite phase into the high resistive martensite phase inside the martensite transition regime. Sharma *et al.* showed that the resistance of the martensite phase is higher than that of the austenite phase in Ni–Mn based Heusler alloys.[53] Below 304 K, the resistivity remains almost constant up to 290 K, as the sample in the pure martensite phase in this temperature range. The drastic change in resistivity inside the MT regime is due to a structural change from the high temperature cubic austenite phase to the low temperature tetragonal $L1_0$ structure, where changes in the Ni–Mn bond length occur, thereby modifying the density of states near the Fermi level.[21,54] The nature of isofield $\rho(T)$ remains the same for heating path like cooling path with a clear thermal hysteresis, which again confirms the first order nature of MT as observed in isofield thermomagnetization data [Fig. 4(a)]. No thermal hysteresis in resistivity is observed when the sample is in the pure austenite or martensite phase. In Fig. 7(a), the points A and B represent the resistivity at 310 K for heating and cooling paths, respectively, for 0 T magnetic field. The higher resistivity of point A than B indicates a higher amount of martensite phase present in the sample at a particular temperature in the heating path. So, the fraction of the austenite and martensite phases is thermal path dependent inside the MT regime. It is also evident from Fig. 7(a) that the nature of $\rho(T)$ remains the same under the application of 8 T magnetic field, except the shift of the thermal hysteresis loop of resistivity toward lower temperatures. This phenomenon is consistent with Fig. 4(d), which confirms that the application of magnetic field stabilizes the austenite phase in the sample. The point C in Fig. 7(a) represents resistivity at 310 K under the application of 8 T magnetic field in the heating mode. So, comparing the points A and C, it can be concluded that, for the same thermal history, the resistivity decreases with the application of the magnetic field at a particular temperature inside the

TABLE I. Comparison of T_{AM}, ΔS_M, RC, and ΔT_{ad} for $Ni_{45}Mn_{44}Sn_{11-x}In_x$ (x = 0, 2, 4) and other Heusler alloys for the change in the 5 T magnetic field in the vicinity of the first order magneto-structural martensite transition.

Sample name	Reference	T_{AM} (K)	ΔS_M (J kg^{-1} K^{-1}) for the change in the 5 T magnetic field	RC (J kg^{-1}) for the change in the 5 T magnetic field	ΔT_{ad} (K) for the change in the 5 T magnetic field
$Ni_{45}Mn_{44}Sn_{11}$	13	264.8	15.0	71.0	−5.1
$Ni_{45}Mn_{44}Sn_9In_2$	26	290.0	17.0	48.0	−3.8
$Ni_{45}Mn_{44}Sn_7In_4$	This work	310.2	17.3	100.8	−7.2
$Ni_{45}Mn_{44}Sn_{10}Al_1$	2	293.0	13.5	36.0	−2.7
$Ni_{45}Mn_{44}Sn_9Al_2$	2	357.0	19.5	13.9	−1.2
$Ni_{50}Mn_{34}In_{16}$	51	240.0	19.0	220	−9
$Ni_{50}Mn_{34}Sn_{16}$	51	220.0	2.0	48	−1
$Ni_{44}Mn_{45}Sn_{11}$	19	245.0	10.1	…	…
$Ni_{43}Mn_{46}Sn_{11}$	19	200.0	10.4	…	…

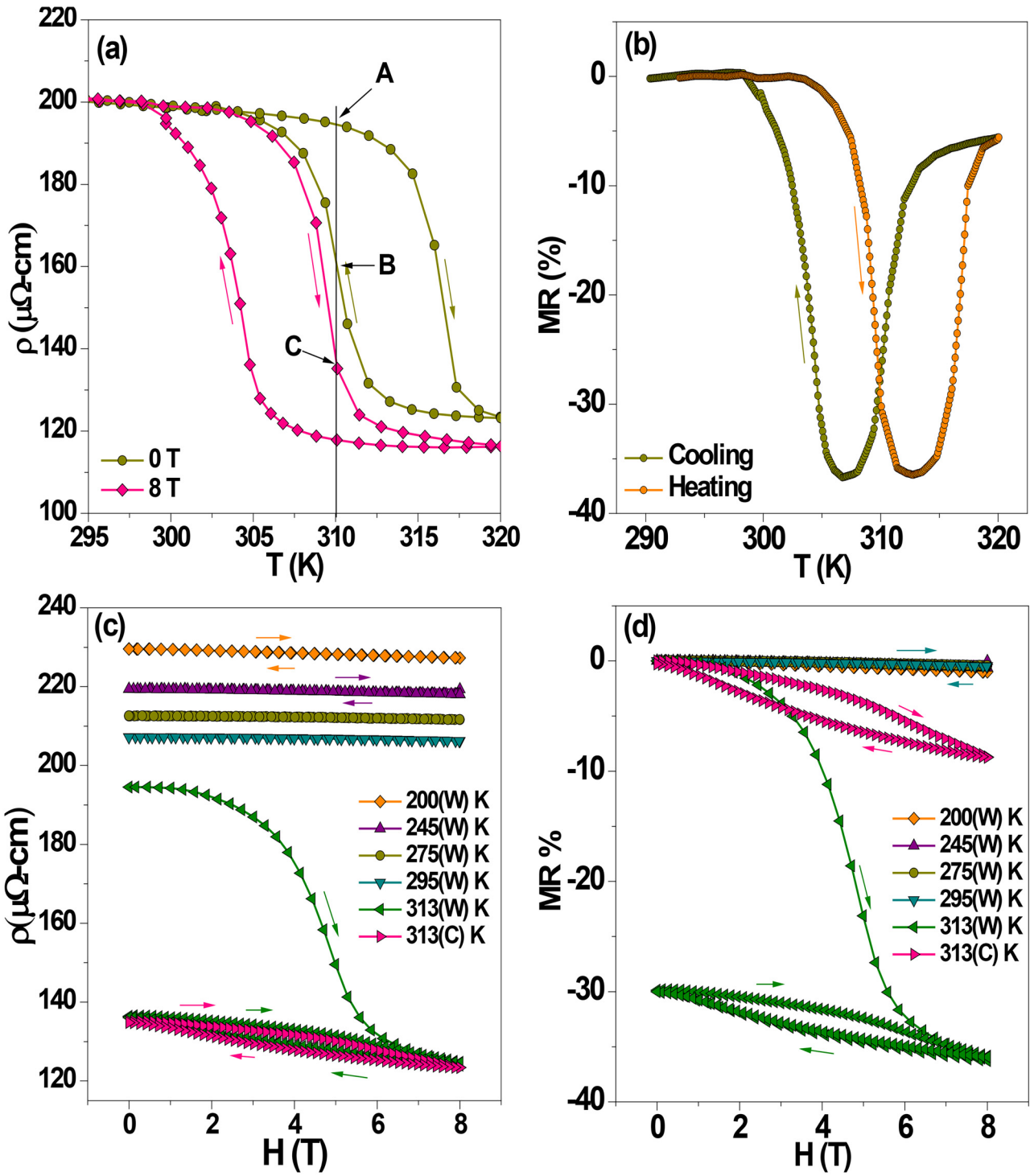

FIG. 7. (a) Temperature dependence of resistivity for cooling and heating paths in the vicinity of the MT regime for 0 T and 8 T magnetic field. (b) MR vs *T* in heating and cooling paths for the change in the magnetic field of 8 T. (c) Isothermal resistivity vs magnetic field at different isothermal conditions in the first quadrant for magnetic field increasing and decreasing paths. (d) MR vs *H* at different isothermal conditions in the first quadrant for magnetic field increasing and decreasing paths.

martensite transition regime. As a result, one can expect large negative magnetoresistance (MR) inside the martensite transition regime. Figure 7(b) shows the plot of MR vs T for the change in 8 T magnetic field for cooling and heating paths. The maximum negative MRs are found to be −36.7% and −36.4% for cooling and heating paths, respectively, for the change in the magnetic field of 8 T. However, to explore the magnetoresistance property of the $Ni_{45}Mn_{44}Sn_7In_4$ Heusler alloy directly, we have recorded magnetic field dependent resistivity [$\rho(H)$] at different isothermal conditions. Figure 7(c) shows $\rho(H)$ data at various temperatures. Now, as the resistivity of the sample at a particular temperature depends on the thermal path inside MT, we have measured the $\rho(H)$ data at 313 K after reaching the respective temperature in two different thermal paths. In the first case, the temperature of the sample is decreased from 320 K to 100 K and then increased to 313 K and subsequently, the magnetic field is applied to record $\rho(H)$ data. The data obtained by this protocol are labeled as 313(W) K. The isothermal $\rho(H)$ data at 200 K, 245 K, 275 K, and 295 K (outside the MT transition regime) are also recorded following this protocol and labeled as 200(W) K, 245(W) K, 275(W) K, and 295(W) K, respectively. In the second case, the temperature of the sample is decreased directly from 320 K to 313 K. The data obtained by this protocol are labeled as 313(C) K. It is observed from Fig. 7(c) that the resistivity of the $Ni_{45}Mn_{44}Sn_7In_4$ alloy at 200(W) K, 245(W) K, 275(W) K, and 295 (W) K decreases with increasing temperature and remains nearly constant with the increase in the magnetic field. This happens because at these temperatures, the sample in the martensite phase tends to loosen its rigidity with increasing temperature but no field induced transition occurs with increasing magnetic field. At 313 (W) K and 313(C) K, the resistivities are 194.5 $\mu\Omega$ cm and 134.7 $\mu\Omega$ cm, respectively, at 0 T magnetic field for the field increasing path, which confirms the presence of a larger amount of the martensite phase fraction for 313(W) K than at 313(C) K in the absence of any magnetic field. It is also observed that the rate of decrease in the resistivity is larger for 313(W) K than at 313(C) K with the increase in the magnetic field because of the higher rate of field induced transformation from the martensite phase to the austenite phase due to the availability of a large amount of the martensite phase at 313(W) K than at 313(C) K. At first, resistivity decreases gradually with the increase in the magnetic field and then rate of decrease in the resistivity increases after 3 T magnetic field. The same phenomenon is seen in isothermal M–H data of Fig. 5(a), where magnetization increases rapidly at the isothermal condition after 3 T magnetic field in the MT regime. The resistivity is the same (123.3 $\mu\Omega$ cm) for 313(W) K and 313(C) K for the application of the magnetic field of 8 T, thereby confirming that field induced transformation from the martensite phase to the austenite phase has been completed at 8 T magnetic field and the sample is in the pure austenite phase. It is observed that the magnetic field decreasing $\rho(H)$ data follow the same path of field increasing data due to the absence of the field induced transition at 200(W) K, 245(W) K, 275(W) K, and 295(W) K, when the sample is in the pure martensite phase. However, a clear magnetic hysteresis between field increasing and decreasing $\rho(H)$ data at 313(W) K and 313(C) K has been noticed, as seen in Fig. 7(c). The resistivity at the field decreasing path is lower than the field increasing path at a particular magnetic field. This implies that the conversion of the low resistive austenite phase into the high resistive martensite phase has not occurred by the same amount due to the withdrawal of the magnetic field at a particular magnetic field. As a result, the austenite phase remains partially arrested in the martensite phase matrix. This phenomenon is consistent with $M(H)$ data inside the MT regime [Fig. 5(a)]. For 313(W) K, the resistivity at 0 T for the field decreasing path is 136.4 $\mu\Omega$ cm, which is lower by 58.1 $\mu\Omega$ cm, than field increasing resistivity data at 0 T. However, the resistivities at 0 T for field increasing and field decreasing paths are the same for 313(C) K, unlike 313(W) K. Figure 7(d) shows MR vs H data at 200(W) K, 245(W) K, 275(W) K, 295(W) K, 313(W) K, and 313(C) K. MR of −0.9% and −0.4% have been observed at 200 (W) K and 275(W) K for the change in the magnetic field of 8 T. However, MR of −36.2% and −8.7% have been noticed at 313(W) K and 313(C) K due to the application of 8 T magnetic field, initially. The maximum MR for the $Ni_{45}Mn_{44}Sn_9In_2$ Heusler alloy was found to be −33% for the change in the 8 T magnetic field at 295 K.[26] So, it can be concluded that MR of the sample increases with the increase in the In content at Sn sites. The subsequent removal of the magnetic field does not affect much in MR, due to the partial arrest of the austenite phase in the martensite phase matrix. So, it is confirmed that field induced conversion, arrested austenite phase, and large MR have been observed only inside the MT regime due to the interplay of austenite and martensite phases. Thus, there must be some connection between MR and field induced austenite phase inside the MT regime, which is responsible for the large MR.

In the following section, we will quantify the amount of the transformed austenite phase inside the MT regime as a function of magnetic field for increasing and decreasing field paths and also show how MR varies with the transformed austenite phase fraction at a particular temperature due to the application of the magnetic field inside the MT regime. For this, we have denoted martensite phase fraction, austenite phase fraction, and field induced austenite phase fraction at a particular magnetic field and temperature as $f_M(T,H)$, $f_A(T,H)$, and $f_{FIA}(T,H)$, respectively. As, due to the application of the magnetic field, some of the martensite phase is transformed into the austenite phase, we can write

$$f_M(T,0) = f_M(T,H) + f_{FIA}(T,H). \tag{7}$$

Since, the summation of the austenite phase and martensite phase is unity at a particular temperature and magnetic field, we can also write

$$f_M(T,H) + f_A(T,H) = 1. \tag{8}$$

To calculate $f_M(T,H)$ and $f_{FIA}(T,H)$, we have used the Landauer equation for two coexisting phases,[55]

$$\sigma(T) = \frac{1}{4}\Big[(3f_A-1)\sigma_A + (3f_M-1)\sigma_M + [\{(3f_A-1)\sigma_A + (3f_M-1)\sigma_M\}^2 + 8\sigma_A\sigma_M]^{\frac{1}{2}}\Big]. \tag{9}$$

Substituting $f_A(T,H)$ by $f_M(T,H)$, we can find $f_M(T,H)$ using Eq. (9), where σ_A and σ_M are the conductivities of austenite and martensite

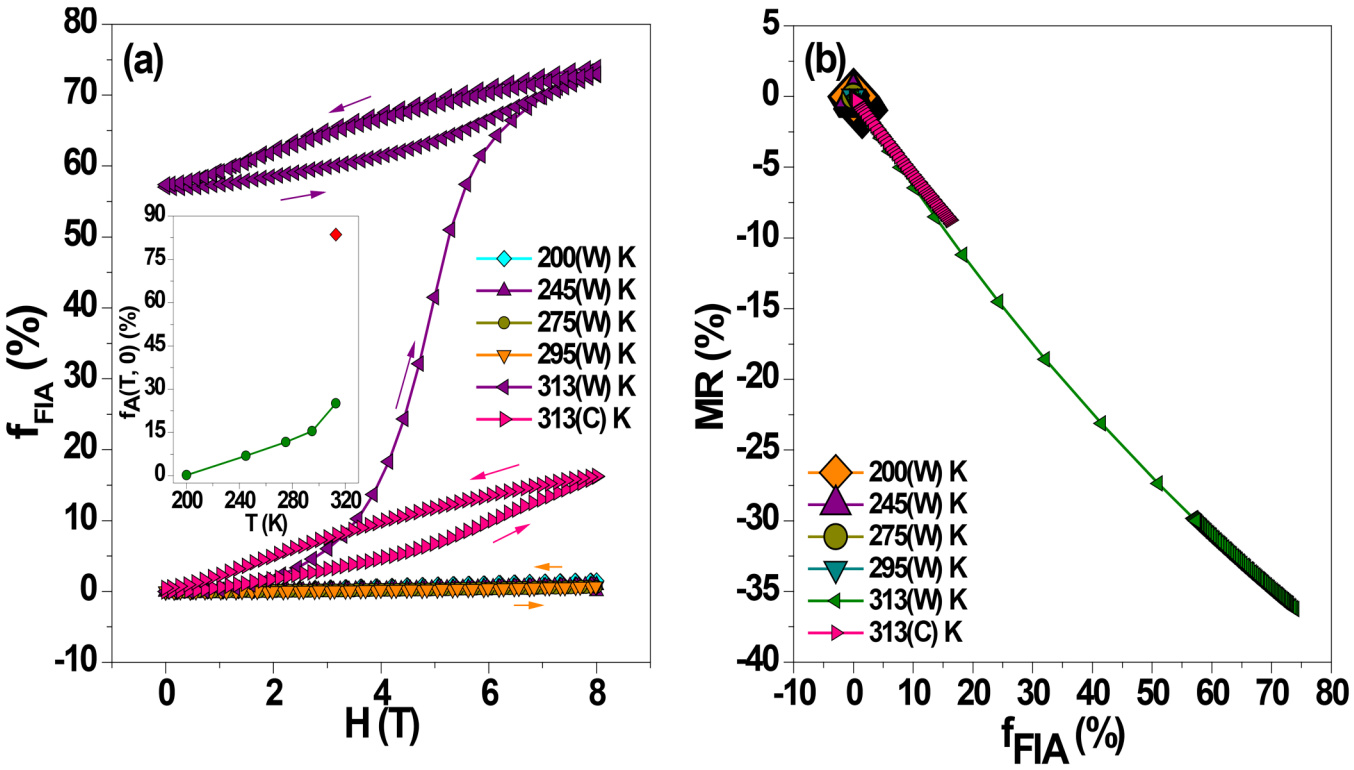

FIG. 8. (a) Field induced austenite phase fraction vs magnetic field at different isothermal conditions for magnetic field increasing and decreasing paths. Inset: red dot denotes the $f_A(T,0)$ at 313(C) K and green dots denote the variation of austenite phase with temperature, when the respective temperature is reached by heating in the absence of any magnetic field. (b) MR vs $f_{FIA}(T,H)$ plots for different isothermal conditions.

phases, respectively. We have taken ρ_M as the resistivity at 0 T from isothermal $\rho(H)$ data at 200(W) K. The resistivity at 8 T from isothermal $\rho(H)$ data at 313(C) K is taken as ρ_A. From the knowledge of $f_M(T,H)$, we can calculate $f_{FIA}(T,H)$ using Eq. (7). Figure 8(a) shows the variation of $f_{FIA}(T,H)$ with magnetic field. It has been observed that $f_{FIA}(T,H)$ remains almost zero for 200(W) K, 245(W) K, 275(W) K, and 295(W) K. But when the temperature is 313(W) K and 313(C) K, $f_{FIA}(T,H)$ increases with the increase in the magnetic field due to the availability of the metastable martensite phase, which can be converted into the austenite phase. At 313(W) K and 313(C) K, for the application of 8 T magnetic field, $f_{FIA}(T,H)$ are found to be 73.9% and 16.2%, respectively. So, the amount of the field induced austenite phase fraction depends on thermal paths at a particular temperature. The inset of Fig. 8(a) shows the variation of the austenite phase present in the sample at 0 T magnetic field with temperature for different thermal path histories, where red dot denotes the $f_A(T,0)$ at 313(C) K and green dots denote the same at 200(W) K, 245(W) K, 275(W) K, 295(W) K, and 313(W) K. The observed austenite phase fractions are 25.0% and 83.6% for 313(W) K and 313(C) K, respectively, when no magnetic field is applied. Variations of $f_M(T,H)$ with magnetic field for different isothermal conditions are also plotted (see Fig. S4 in the supplementary material). It is observed from Figs. 7(d) and 8(a) that MR is maximum at 313(W) K when $f_{FIA}(T,H)$ is maximum, and it is also noticed that the nature of $f_{FIA}(T,H)$ vs H and MR vs H are similar with an inverted configuration. So, there must be some correlation between MR and $f_{FIA}(T,H)$. Figure 8(b) shows MR vs $f_{FIA}(T,H)$ plots for different isothermal conditions, which concludes that MR is maximum when f_{FIA} is maximum for the change in the 8 T magnetic field. So, it is confirmed that MR of these kinds of Heusler alloys, having first order magnetostructural martensite transition depends on the availability of the metastable martensite phase, which can be transformed into the austenite phase with the application of the magnetic field. For this reason, MR is negligible for 200(W) K, 200(W) K, 245(W) K, 275(W) K, and 295(W) K, as the available metastable martensite phase fraction is negligibly small at these temperatures, though a high amount of the stable martensite phase is available at these temperatures. So, the $Ni_{45}Mn_{44}Sn_7In_4$ alloy can be used as a high and low resistive material inside MT by varying the magnetic field only.

IV. CONCLUSIONS

We have carried out extensive studies on the compositional, structural, calorimetric, magnetic, electronic-transport, and magneto-transport properties of the $Ni_{45}Mn_{44}Sn_7In_4$ Heusler alloy.

From XRD, it has been confirmed that the sample has a tetragonal $L1_0$ martensite phase at room temperature. First-order martensite transition has been observed from the isofield thermo-magnetic and electronic-transport data. The austenite and martensite phase fractions at a particular temperature depend on their thermal path history. The austenite phase fraction at a particular temperature is larger, when the respective temperature is reached by cooling from higher temperatures. The observed austenite phase fractions are 25.0% and 83.6% for 313(W) K and 313(C) K, respectively, in the absence of the magnetic field. The field induced conversion of the martensite phase into the austenite phase has been noticed from field dependent magnetization and resistivity data at isothermal conditions by the application of magnetic field inside the martensite transition regime. As a result, magnetization increases and resistivity decreases rapidly beyond 3 T magnetic field. So, the magnetization and resistivity of the sample can be manipulated by the application of the magnetic field only, at a particular temperature inside MT. However, the subsequent withdrawal of the magnetic field does not bring back same amount of the martensite phase due to the partial arrest of the austenite phase. As a consequence, the magnetization and resistivity of the field decreasing path remain higher and lower, respectively, with respect to the field increasing path. The MR of the $Ni_{45}Mn_{44}Sn_7In_4$ Heusler alloy entirely depends on the availability of the metastable martensite phase, which can be converted into the austenite phase by the application of the magnetic field. The maximum MR is found to be −36.2% for the change in 8 T magnetic field when the field induced austenite phase fraction (f_{FIA}) is 73.9%. ΔS_M, RC, and ΔT_{ad} are found to be 17.5 J $kg^{-1}K^{-1}$, 100.8 J/kg, and −7.2 K, respectively, for the change in 5 T magnetic field near 315 K, which is very close to room temperature. Comparing with our previously reported $Ni_{45}Mn_{44}Sn_{11-x}In_x$ (x = 0, 2) Heusler alloys,[13,26] the large values of ΔS_M, RC, and ΔT_{ad} in the vicinity of room temperature make $Ni_{45}Mn_{44}Sn_7In_4$ Heusler alloy a much promising and better candidate as a magnetic refrigerant.

SUPPLEMENTARY MATERIAL

See the supplementary material for the determination of the Curie temperature of the martensite phase (T_C^M) and Curie temperature of the austenite phase (T_C^A), shift of the direct martensite temperature (T_{AM}) and reverse martensite temperature (T_{MA}), difference of magnetization at isothermal conditions inside MT and variation of the martensite phase fraction as a function of magnetic field at different constant temperatures.

ACKNOWLEDGMENTS

The authors thank Dr. R. Rawat for electronic transport measurements. This work is funded by the UGC through (Reference No. 17-06/2012(i)EU-V). T.K.N. would like to acknowledge financial assistance of the project grant funded by the UGC-DAE Consortium for Scientific Research (Reference No. CSR-IC-257/2017-18/1338) to carry out some experiments. D.M. acknowledges funding from the Technical Research Center, Department of Science and Technology, Government of India (Grant No. AI/1/62/IACS/2015) and Science and Engineering Research Board, Government of India (Grant No. SRG/2019/000387).

DATA AVAILABILITY

The data that support the findings of this study are available within the article and its supplementary material.

REFERENCES

[1]B. F. Yu, Q. Gao, B. Zhang, X. Z. Meng, and Z. Chen, Int. J. Refrig. **26**, 622 (2003).
[2]T. Chabri, A. M. Awasthi, K. Ghosh, A. Venimadhav, and T. K. Nath, Mater. Res. Express **5**, 086511 (2018).
[3]O. Tegus, E. Brück, L. Zhang, Dagula, K. H. J. Buschow, and F. R. de Boer, Phys. B Condens. Matter **319**, 174 (2002).
[4]Y. Q. Zhang and Z. D. Zhang, J. Alloys Compd. **365**, 35 (2004).
[5]S. A. Nikitin, G. Myalikgulyev, A. M. Tishin, M. P. Annaorazov, K. A. Asatryan, and A. L. Tyurin, Phys. Lett. A **148**, 363 (1990).
[6]L. Pareti, M. Solzi, F. Albertini, and A. Paoluzi, Eur. Phys. J. B **32**, 303 (2003).
[7]G. V. Brown, J. Appl. Phys. **47**, 3673 (1976).
[8]A. R. Dinesen, S. Linderoth, and S. Mørup, J. Phys. Condens. Matter **17**, 6257 (2005).
[9]A. Fujita, S. Fujieda, Y. Hasegawa, and K. Fukamichi, Phys. Rev. B **67**, 104416 (2003).
[10]F.-X. Hu, B.-G. Shen, J.-R. Sun, Z.-H. Cheng, G.-H. Rao, and X.-X. Zhang, Appl. Phys. Lett. **78**, 3675 (2001).
[11]V. K. Pecharsky and J. K. A. Gschneidner, Phys. Rev. Lett. **78**, 4494 (1997).
[12]O. Tegus, E. Brück, K. H. J. Buschow, and F. R. de Boer, Nature **415**, 150 (2002).
[13]T. Chabri, A. Venimadhav, and T. K. Nath, Intermetallics **102**, 65 (2018).
[14]T. Chabri, A. Venimadhav, and T. K. Nath, AIP Conf. Proc. **1832**, 030008 (2017).
[15]J. Du, Q. Zheng, W. J. Ren, W. J. Feng, X. G. Liu, and Z. D. Zhang, J. Phys. D Appl. Phys. **40**, 5523 (2007).
[16]J. Liu, T. Gottschall, K. P. Skokov, J. D. Moore, and O. Gutfleisch, Nat. Mater. **11**, 620 (2012).
[17]V. D. Buchelnikov and V. V. Sokolovskiy, Phys. Met. Metallogr. **112**, 633 (2011).
[18]Y. Sutou, Y. Imano, N. Koeda, T. Omori, R. Kainuma, K. Ishida, and K. Oikawa, Appl. Phys. Lett. **85**, 4358 (2004).
[19]Z. D. Han, D. H. Wang, C. L. Zhang, H. C. Xuan, B. X. Gu, and Y. W. Du, Appl. Phys. Lett. **90**, 042507 (2007).
[20]R. Kainuma, Y. Imano, W. Ito, Y. Sutou, H. Morito, S. Okamoto, O. Kitakami, K. Oikawa, A. Fujita, T. Kanomata, and K. Ishida, Nature **439**, 957 (2006).
[21]S. Y. Yu, Z. H. Liu, G. D. Liu, J. L. Chen, Z. X. Cao, G. H. Wu, B. Zhang, and X. X. Zhang, Appl. Phys. Lett. **89**, 162503 (2006).
[22]K. Koyama, K. Watanabe, T. Kanomata, R. Kainuma, K. Oikawa, and K. Ishida, Appl. Phys. Lett. **88**, 132505 (2006).
[23]S. Y. Yu, L. Ma, G. D. Liu, Z. H. Liu, J. L. Chen, Z. X. Cao, G. H. Wu, B. Zhang, and X. X. Zhang, Appl. Phys. Lett. **90**, 242501 (2007).
[24]T. Chabri, A. Venimadhav, and T. K. Nath, J. Magn. Magn. Mater. **466**, 385 (2018).
[25]M. Modak, M. K. Ray, S. Mondal, B. Maji, K. Bagani, A. Bhattacharyya, and S. Banerjee, J. Phys. D Appl. Phys. **53**, 205301 (2020).
[26]T. Chabri, A. Ghosh, S. Nair, A. M. Awasthi, A. Venimadhav, and T. K. Nath, J. Phys. D Appl. Phys. **51**, 195001 (2018).
[27]F. Scheibel, T. Gottschall, A. Taubel, M. Fries, K. P. Skokov, A. Terwey, W. Keune, K. Ollefs, H. Wende, M. Farle, M. Acet, O. Gutfleisch, and M. E. Gruner, Energy Technol. **6**, 1397 (2018).
[28]S. Chatterjee, S. Giri, S. Majumdar, and S. K. De, Phys. Rev. B **77**, 012404 (2008).

[29]S. Chatterjee, S. Giri, S. Majumdar, and S. K. De, Phys. Rev. B **77**, 224440 (2008).
[30]H. C. Xuan, Y. X. Zheng, S. C. Ma, Q. Q. Cao, D. H. Wang, and Y. W. Du, J. Appl. Phys. **108**, 103920 (2010).
[31]Z. Guo, L. Pan, M. Y. Rafique, X. Zheng, H. Qiu, and Z. Liu, J. Alloys Compd. **577**, 174 (2013).
[32]Q. Tao, Z. D. Han, J. J. Wang, B. Qian, P. Zhang, X. F. Jiang, D. H. Wang, and Y. W. Du, AIP Adv. **2**, 042181 (2012).
[33]T. Krenke, M. Acet, E. F. Wassermann, X. Moya, L. Mañosa, and A. Planes, Phys. Rev. B **72**, 014412 (2005).
[34]M. Ye, A. Kimura, Y. Miura, M. Shirai, Y. T. Cui, K. Shimada, H. Namatame, M. Taniguchi, S. Ueda, K. Kobayashi, R. Kainuma, T. Shishido, K. Fukushima, and T. Kanomata, Phys. Rev. Lett. **104**, 176401 (2010).
[35]Y. Imry and M. Wortis, Phys. Rev. B **19**, 3580 (1979).
[36]J. Chen, Z. Han, B. Qian, P. Zhang, D. Wang, and Y. Du, J. Magn. Magn. Mater. **323**, 248 (2011).
[37]T. Krenke, M. Acet, E. F. Wassermann, X. Moya, L. Mañosa, and A. Planes, Phys. Rev. B **73**, 174413 (2006).
[38]Z. D. Han, D. H. Wang, C. L. Zhang, S. L. Tang, B. X. Gu, and Y. W. Du, Appl. Phys. Lett. **89**, 182507 (2006).
[39]W. Wang, J. Yu, Q. Zhai, Z. Luo, and H. Zheng, J. Magn. Magn. Mater. **346**, 103 (2013).
[40]C. Jiang, Y. Muhammad, L. Deng, W. Wu, and H. Xu, Acta Mater. **52**, 2779 (2004).
[41]J. Liu, H. X. Zheng, M. X. Xia, Y. L. Huang, and J. G. Li, Scr. Mater. **52**, 935 (2005).
[42]Z. D. Han, D. H. Wang, C. L. Zhang, H. C. Xuan, J. R. Zhang, B. X. Gu, and Y. W. Du, Mater. Sci. Eng. B **157**, 40 (2009).
[43]S. Aksoy, T. Krenke, M. Acet, E. F. Wassermann, X. Moya, L. Mañosa, and A. Planes, Appl. Phys. Lett. **91**, 241916 (2007).
[44]P. A. Bhobe, K. R. Priolkar, and P. R. Sarode, J. Phys. Condens. Matter **20**, 015219 (2008).
[45]T. Krenke, E. Duman, M. Acet, E. F. Wassermann, X. Moya, L. Mañosa, and A. Planes, Nat. Mater. **4**, 450 (2005).
[46]S. Das, J. S. Amaral, and V. S. Amaral, J. Phys. D Appl. Phys. **43**, 152002 (2010).
[47]W. Cui, W. Liu, and Z. Zhang, Appl. Phys. Lett. **96**, 222509 (2010).
[48]M. Balli, D. Fruchart, D. Gignoux, and R. Zach, Appl. Phys. Lett. **95**, 072509 (2009).
[49]L. Caron, Z. Q. Ou, T. T. Nguyen, D. T. Cam Thanh, O. Tegus, and E. Brück, J. Magn. Magn. Mater. **321**, 3559 (2009).
[50]A. M. Tishin and Y. I. Spichkin, *The Magnetocaloric Effect and its Applications* (Institute of Physics Publishing, Bristol, 2003).
[51]V. K. Sharma, M. K. Chattopadhyay, K. Ravi, G. Tapas, T. Pragya, and S. B. Roy, J. Phys. Condens. Matter **19**, 496207 (2007).
[52]Y. Zhang, Q. Zheng, W. Xia, J. Zhang, J. Du, and A. Yan, Scr. Mater. **104**, 41 (2015).
[53]V. K. Sharma, M. K. Chattopadhyay, K. H. B. Shaeb, A. Chouhan, and S. B. Roy, Appl. Phys. Lett. **89**, 222509 (2006).
[54]P. A. Bhobe, K. R. Priolkar, and P. R. Sarode, Phys. Rev. B **74**, 224425 (2006).
[55]R. Landauer, J. Appl. Phys. **23**, 779 (1952).